Dalton Transactions

Accepted Manuscript

ROYAL SOCIETY OF CHEMISTRY

www.rsc.org/dalton

Dalton Transactions

Dalton Transactions

Dynamic Article Links ►

Cite this: DOI: 10.1039/c0xx00000x

www.rsc.org/xxxxxx

PAPER

Structural and magnetic properties of some lanthanide (Ln= Eu(III), Gd(III) and Nd(III)) cyanoacetate polymers: Field-induced slow magnetic relaxation in the Gd and Nd substitutions.

A. Arauzo[a, b], A. Lazarescu[c], S. Shova[c, f], E. Bartolomé[d], R. Cases[b], J. Luzón[b,e], J. Bartolomé[b], C. Turta[c]

Received (in XXX, XXX) Xth XXXXXXXXX 20XX, Accepted Xth XXXXXXXXX 20XX
DOI: 10.1039/b000000x

The lanthanide(III) cyanoacetate complexes of formula $\{[Ln_2(CNCH_2COO)_6(H_2O)_4]\cdot 2H_2O\}_n$, where Ln= Eu (**1**), Gd (**2**), Nd (**3**), have been prepared and characterized by X-ray diffraction analysis. Complexes **1**, **2** are isostructural and differ from the binding scheme of neodymium compound **3**, structurally described earlier. In all cases, the cyano group of the cyanoacetate ligand is not coordinated to the lanthanide cation. The carboxylic groups exhibit different binding modes: 2-bidentate-chelating, 2-bidentate and 2-tridentate-chelating bridging for **1** and **2**; 4-bidentate and 2-tridentate-chelating bridging for complex **3**. The Eu compound **1** shows field induced paramagnetism, as expected for a non-magnetic ground state with mixing from higher states. Combining the dc magnetization and luminescence measurements the spin-orbit coupling constant λ=343±4 cm^{-1} was found, averaged over the two different sites for Eu in the lattice. In Gd complex **2**, a crystal field splitting of D/k_B=-0.11±0.01 K has been found for the S=7/2 multiplet of the Gd(III) ion. No slow relaxation at H=0 is observed because the low anisotropy barrier allows fast spin reversal through classical processes. The application of an external magnetic field induces two slow relaxation processes. It is argued that the first relaxation rate is caused by Resonant Phonon Trapping (RPT) mechanism, while the second, slower one is due to the lifting of the Kramers degeneracy on the ground state. For compound **3** heat capacity and dc susceptibility measurements indicate that at very low temperature the ground state Kramers doublet has strong single ion anisotropy. The energy to the next excited doublet Δ_{ZFS}/k_B= 104 K has been calculated by *ab initio* calculation methods. The g* tensor has also been calculated, showing that it has predominant anisotropy along the z axis, and there is an important transversal component. At H=0 quantum tunnelling is an effective mechanism in producing a fast relaxation to equilibrium at temperature above 1.8 K. The dipolar or exchange interactions and a sizable transverse anisotropy component in the ground state enhance the quantum tunneling probability. Under an external applied field, two slow relaxation processes appear: above 3 K the first relaxation mechanism is of Orbach type, with an activation energy U/k_B=27 K; the slower one is caused by the direct relaxation process from the ground state to the Kramers split levels by the applied field.

1. Introduction

The synthesis and characterization of rare earth coordination polymers are of intense current interest due to the unique properties of the various 4f ions and to their potential applications as essential components in the production of new magnetic and optical materials [1, 2].

Recently, there have been described numerous lanthanide complexes containing different organic ligands [3], acting as building blocks in the construction of infinite architectures.

Among these ligands, the multidentate carboxylates are most investigated. Certain choices of carboxylic ligands coupled with the lanthanide ions may lead to the formation of new complexes of different dimensionality and unique properties [4]. To date, the lanthanide(III) complexes with cyanoacetic acid have received less attention [5]. Our studies concerning the use of cyanoacetic acid with both O- and N- possible donor atoms as a ligand towards 3d [6] and 4f [7] cations have shown that different polymeric structures can be obtained due to the coordination modes adopted by this ligand. In copper(II) cyanoacetate complex the cyano-group participates in the coordination to the metal ion, whereas in neodymium(III) complex the coordination is achieved by oxygen atoms only [6, 7].

In this paper, we continue the structural study of lanthanide(III) cyanoacetate bridged complexes in order to investigate the coordination abilities of lanthanide(III) ions in the construction of polymeric structures and their magnetic behavior. We have chosen complexes with composition $\{[Ln_2(CNCH_2COO)_6(H_2O)_4]\cdot 2H_2O\}_n$, where Ln= Eu (**1**) Gd (**2**),

[a] *Servicio de Medidas Físicas. Universidad de Zaragoza, Pedro Cerbuna 12, 50009 Zaragoza, Spain.*
[b] *Instituto de Ciencia de Materiales de Aragón, CSIC-Universidad de Zaragoza, Pedro Cerbuna 12, 50009 Zaragoza, Spain.*
[c] *Institute of Chemistry, Academy of Sciences of Moldova, Academiceskaya 3, MD-2028,Chisinau, Moldova.*
[d] *Escola Universitària Salesiana de Sarrià (EUSS), Passeig Sant Joan Bosco 74, 08017-Barcelona, Spain.*
[e] *Centro Universitario de la Defensa. Academia General Militar, Zaragoza, Spain.*
[f] *"Petru Poni" Institute of Macromolecular Chemistry, Alea Gr. Ghica Voda 41A, 700487 Iasi, Romania*

and Nd (**3**). The synthesis and X-ray structure determination of complexes (**1**) and (**2**) is also presented, whereas that of complex (**3**) was already reported in a previous work [7]. We note here that the Nd complex is not isostructural to the Gd and Eu ones, but is closely related. This family of compounds supply Lanthanide substituted polymers with tri-capped trigonal prism coordination and, consequently, similar ligand field interactions. A comparative study of their magnetic properties under dc and ac magnetic fields allow, in this case, to deepen in the understanding of the peculiar Single Ion Magnet properties of the R=Gd and Nd substitutions. The Eu compound serves as a reference compound to determine the lattice heat capacity, an essential item in our work. Then, both Gd and Nd, due to different reasons, low anisotropy in the first case, and orthorhombic symmetry in the second, show field induced slow relaxation.

Indeed, there is currently much interest in the capacity of Ln(III) compounds to show slow relaxational behavior. Many examples based on Ln=Dy substitution have provided excellent examples as Single Ion Magnets (SIM) [8], Single Molecule Magnets (SMM) [9] or Single Chain Magnets (SCM) [10], in all cases because of the extremely high uniaxial single ion anisotropy of Dy.

Actually, in most SMM systems, slow relaxation arises from the hindering to spin reversal by a uniaxial magnetic anisotropy. The combination of a high spin ground state and a magnetic anisotropy energy barrier with respect to reversal of the spin gives as a result magnetic bistability. The relaxation barrier must be large enough to ensure stability of the moment orientation to classical and thermally activated quantum fluctuations.

Attention has shifted in the last years from giant clusters with the highest possible ground state spin and negative axial anisotropy to more simple, SIMs, with the aim of understanding magnetic relaxation processes. New fascinating phenomena are an active research topic, as slow magnetic relaxation induced by easy-plane anisotropy [11], field-induced or field-influenced slow magnetic relaxation in mononuclear transition metal compounds [12] and lanthanide compounds [13].

Gd(III) compounds have a very low anisotropy, which has even been considered negligible in many studies. However, at very low temperature the anisotropy can be effective enough to show slow relaxation as in GdW_n compounds [14]. In spite of this example, no slow relaxational behavior has been reported on the Gd substitutions of series like $[Ln(BPDC)_{1.5}(DMF)(H_2O)_2].2H_2O$, for example, which showed clear slow relaxation for other Ln(III), like Tb or Dy [15].

With these antecedents, the observation of slow relaxation in $[Gd_2(fum)_3(H_2O)_4].3H_2O$ under an external applied field was quite unexpected [13, 16]. In the present work we show that in compound **2** the application of an external field induces a slow relaxation process.

Besides, because of the very low anisotropy energy, low Gd-Gd interaction and high spin moment, Gd complexes are finding their place as potential very low temperature refrigerators by means of their large magnetocaloric effect (MCE) [17]. The figures of merit for this application of complex **2** are analyzed below.

On the other hand, Nd complexes, which may show strong anisotropy, have hardly been explored. In fact, the Nd(III) ion may have a sufficiently high anisotropy to create a hindering barrier to magnetic moment reversal and give rise to slow relaxational behaviour. Otherwise to Dy, where the anisotropy tensor is usually predominant in one direction, the Nd g^*-tensor may have large transversal components, therefore giving the possibility to explore their influence on the dynamical behavior of the Nd(III) as a SIM.

Indeed, the Nd(III) ion has been included in 3d/Nd clusters in the quest for SMMs, but just a few cases of slow relaxation have been reported: in a $[Mn_4Nd_2]$ cluster, a non-zero $\chi''(T, \omega)$ was detected at low temperature [18], which was associated to the presence of the neodymium light rare earth, and in $[Mn_{10}Nd_4]$ [19] and $[Mn_{11}Nd_4]$ [20] asymmetric clusters, where the same feature was observed. Slow relaxation in Ni/Nd Single Chain Magnet has been reported in just one case [21]. In all these other examples the neodymium atom plays a secondary role, increasing the anisotropy to some extent. However, the role of Nd(III) as Single Ion Magnet is not clear. Recently slow relaxation induced by an applied field has been observed in $[NdCo(bpdo)(H_2O)4(CN)6].3H_2O$ [22], a result that has incited us to study this effect in compound **3**.

Therefore, the static and dynamic magnetic behavior under a low-frequency ac field of the compounds $\{[Ln_2(CNCH_2COO)_6(H_2O)_4]\cdot 2H_2O\}_n$, where Ln= Eu (**1**), Gd (**2**), and $\{[Nd_2(CNCH_2COO)_6 (H_2O)_4]\cdot 2H_2O\}_n$ (**3**), structurally described by us earlier [7], have been studied in this work.

2. Experimental

2.1. Synthesis

All reagents of reagent grade were purchased commercially and used without further purification. Reaction of lanthanide Eu(III) or Gd(III), oxides with cyanoacetic acid in molar ratio 1:3 in water solution leads to polymeric complexes with the composition $\{[Ln_2(CNCH_2COO)_6 (H_2O)_4]\cdot 2H_2O\}_n$, where Ln= Eu (**1**), Gd (**2**). Complexes are stable colorless crystalline solids and can be stored in a dry atmosphere at room temperature for a long time. These complexes readily dissolve in water but are insoluble in organic solvents such as acetone, acetonitrile, benzene, methanol, and other common non-polar solvents.

$\{[Eu_2(CNCH_2COO)_6 (H_2O)_4]\cdot 2H_2O\}_n$ (**1**). The solution of cyanoacetic acid (0.51 g, 6 mmol) in water (10 ml) was added to 0.36 g (1 mmol) of Eu_2O_3. The resulting solution was passed through a glass filter after stirring. The filtrate was stored at room temperature for some weeks, whereupon colorless crystals of the product suitable for X-ray analysis appeared. The crystals were collected by filtration and dried under reduced pressure. Yield: 48 %. Anal. found (calc.)%: for $\{C_9H_{12}N_3O_9Eu\}_n$, C, 23.57 (23.60); H, 2.59(2.62); N 9.14(9.18); Gd, 33.10(33.18). IR data (Nujol, cm^{-1}): 3500br, 3340br, 3270br, 2265sh, 1630m, 1575s, 1560m, 1425s, 1255s, 1180m, 955w, 935m, 915m, 710m, 610m, 575m, 510w, 490m.

$\{[Gd_2(CNCH_2COO)_6 (H_2O)_4]\cdot 2H_2O\}_n$ (2). The complex was prepared in the same way, as for **1**, using 0.51 g (6 mmol) of cyanoacetic acid and 0.35 g (1 mmol) of gadolinium(III) oxide instead of europium(III) oxide. Yield: 52 %. Anal. found (calc.)%: for $\{C_9H_{12}N_3O_9Gd\}_n$, C, 23.29 (23.33); H, 2.53(2.59); N 9.02(9.07); Gd, 33.83(33.94). IR data (Nujol, cm^{-1}): 3545br, 3430br, 3250br, 2265sh, 1705s, 1600vs, 1580s, 1545s, 1410s, 1264m, 1195m, 955w, 930m, 915m, 700m, 570m, 515m.

$\{[Nd_2(CNCH_2COO)_6 (H_2O)_4]\cdot 2H_2O\}_n$ (**3**). This complex was prepared according to ref. [7].

2.2. Physical measurements details

Elemental analyses (C, H, N) were performed on an Elemental Analyzer vario EL(III). The metal contents in the complexes was determined gravimetrically as stable oxide by precipitating lanthanide ions with ammonium hidroxide. IR spectra of polycrystalline samples was recorded on a Perkin Elmer spectrum 100 FT IR Spectrometer in the range 4000-400 cm^{-1}.

Table 1. Crystallographic data, details of data collection and structure refinement parameters for compound **1** and **2**.

Compound	**1**	**2**
Empirical formula	$C_{18}H_{24}Eu_2N_6O_{18}$	$C_{18}H_{24}Gd_2N_6O_{18}$
Molecular weight	916.35	926.93
Temperature (K)	293	100
Wavelength (Å)	MoKα; 0.71073	MoKα; 0.71073
Crystal system	triclinic	triclinic
Space group	$P\bar{1}$	$P\bar{1}$
a (Å)	9.2907(4)	9.2400(4)
b (Å)	10.2235(4)	10.1910(4)
c (Å)	16.6685(6)	16.5190(7)
α (°)	91.619(3)	91.341(2)
β (°)	91.911(3)	91.921(2)
γ (°)	113.207(4)	113.132(2)
V (Å^3)	1452.84(10)	1428.51(10)
Z	4	4
D_{calc} (g /cm^3)	2.095	2.155
μ (mm^{-1})	4.367	4.694
Reflections collected/unique	10382/5916 [R_{int} = 0.0211]	9653/5356 [R_{int} = 0.0544]
Crystal size (mm)	0.20×0.20×0.15	0.25×0.25×0.20
R_1[a]	0.0235	0.0500
wR_2[b]	0.0552	0.1413
GOF[c]	1.013	1.065
$\Delta\rho_{max}$ and $\Delta\rho_{min}$ (eÅ^{-3})	1.00 and -0.71	1.37 and -2.25

[a] $R_1 = \Sigma||F_o| - |F_c||/\Sigma|F_o|$, [b] $wR_2 = \{\Sigma[w\,(F_o^2 - F_c^2)^2]\,/\Sigma[w(F_o^2)^2]\}^{1/2}$.
[c] GOF = $\{\Sigma[w(F_o^2 - F_c^2)^2]\,/(n-p)\}^{1/2}$, where n is the number of reflections and p is the total number of parameters refined.

Fluorescence emission spectra were obtained at room temperature (RT) and 77 K, Liquid Nitrogen Temperature (LNT), by exciting the samples with a 1000 W ORIEL 66187 tungsten halogen lamp and a double 0.22 m SPEX 1680B monochromator. For the emission spectra, the excitation was carried out at 402 nm. Fluorescence emission was detected using a 0.5 JARREL-ASH monochromator with a Hamamatsu R928 photomultiplier tube. All optical spectroscopy measurements were corrected from the system response.

The dc magnetization and ac susceptibility of powdered samples of the **1**, **2** and **3** complexes were measured, from 1.8 K to 300 K, using a Quantum Design superconducting quantum interference device (SQUID) magnetometer. Additional ac measurements were also done on Nd compound **3**, at fixed temperatures in the range 1.9< T< 10 K, with an excitation field of 4 Oe, at dc fields in the range 0< H< 50 kOe, while sweeping the frequency 10< f< 10000 Hz, in a Quantum Design PPMS ACMS magnetometer. Measurements on powdered samples were performed with the addition of Daphne oil, introduced to fix the grains at low temperatures.

Heat capacity $C(T)$ under different applied fields (0-30 kOe) was measured on a pressed powder pellet fixed with Apiezon N grease, using the same PPMS.

3. Structural characterization

3.1. IR spectrography

The IR spectra showed the characteristic absorptions corresponding to the presence of the cyanoacetate ligand in the complexes. The cyanoacetate compounds display the absorption

Table 2. Selected bond distances (Å) in gadolinium complex $[Gd_2(CNCH_2COO)_6\,(H_2O)_4]\cdot 2H_2O$.

Gd1-O10^{1}	2.411(6)	Gd1-O2*w*	2.406(6)	Gd1-O8	2.381(6)
Gd1-O2	2.555(6)	Gd1-O1*w*	2.429(6)	Gd1-O3	2.401(6)
Gd1-O11	2.346(6)	Gd1-O1	2.456(6)	Gd1-O4	2.819(6)
Gd2-O3*w*	2.420(6)	Gd2-O7^{2}	2.467(6)	Gd2-O8^{2}	2.814(6)
Gd2-O12	2.364(6)	Gd2-O4	2.420(6)	Gd2-O6	2.523(6)
Gd2-O9	2.305(6)	Gd2-O5	2.524(6)	Gd2-O4*w*	2.397(6)

Symmetry transformations for equivalent atoms:
[1)] *x-1,y,z;* [2)] *x+1,y,z*

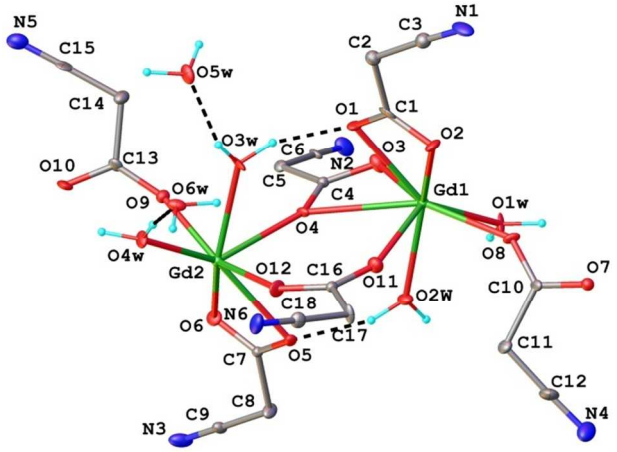

Fig. 1. The structure of $[Gd_2(CNCH_2COO)_6(H_2O)_4]\cdot 2H_2O$ asymmetric unit in **2**.

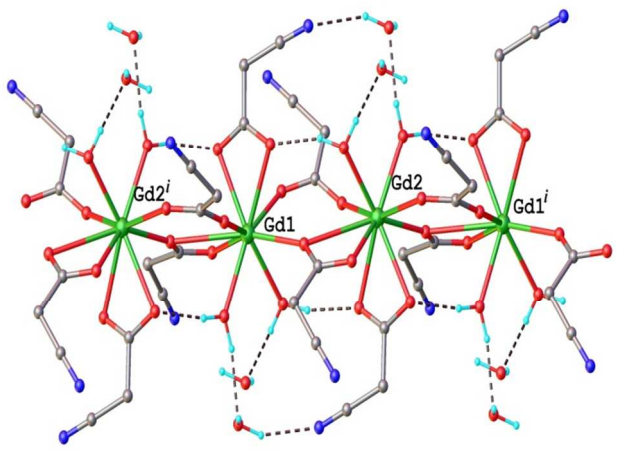

Fig. 2. The structure of one-dimensional coordination polymer $\{[Gd_2(CNCH_2COO)_6(H_2O)_4]\cdot 2H_2O\}_n$.

band at 2265 cm^{-1}, attributed to the ν(C≡N) vibrations [23]. This band did not change its position in the complex, suggesting the non-coordination of the cyano group to the metal. The bands assigned to the coordinated carboxyl groups ($\nu_{as,s}$) are located at 1580 and 1410 cm^{-1} respectively. The presence of water molecules is confirmed by the IR absorption at ~(3545-3250 cm^{-1}) and ~1600 cm^{-1} due to ν(OH) and δ(HOH) vibration modes, respectively.

3.2. X-ray crystallography

Crystallographic measurements for **1** and **2** were carried out with an Oxford-Diffraction XCALIBUR E CCD diffractometer equipped with graphite-monochromated Mo-K_α radiation. The crystals were placed at 40 mm from the CCD detector. The unit cell determination and data integration were carried out using the CrysAlis package of Oxford Diffraction [24]. The absorption corrections were introduced by semiempirical methods based on equivalent reflections. The structures were solved by direct methods using SHELXS-97 [25] and refined by full-matrix least-squares on Fo² with SHELXL-97 [26] with anisotropic displacement parameters for non-hydrogen atoms. All H atoms attached to carbon were introduced in idealized positions (d_{CH}=0.96 Å) using the riding model with their isotropic displacement parameters fixed at 120 % of their riding atom. Positional parameters of the H (water) atoms were obtained from difference Fourier syntheses and verified by the geometric parameters of the corresponding hydrogen bonds. The main crystallographic data together with refinement details are summarised in Table 1. Selected bond lengths and bond angles are given in Table 2.

CCDC-955419 (**1**) and CCDC-955420 (**2**) contain the supplementary crystallographic data for this contribution.

The X-ray studies have demonstrated that compounds **1** and **2** have a similar composition and are isostructural. As an example, the structure of **2** is presented and discussed below. The perspective view of a neutral $[Gd_2(CNCH_2COO)_6(H_2O)_4]\cdot 2H_2O$ asymmetric unit, together with the numbering scheme and selected values of interatomic distances, is presented in Fig. 1 and Table 2.

The tri-capped trigonal prism coordination, with nine oxygen atoms surrounding each Gd atom; seven oxygen atoms originating from carboxylate groups, and two from water molecules. The values of the Gd-O distances are in the range between 2.819(6) and 2.305(6) Å. The two Gd sites are non-equivalent, differing in the actual Gd-O distances (Fig. S.1).. The carboxylate ligands adopt different coordination modes, so that two of them are coordinated as bidentate-chelating ligands, while the remaining four act as bidentate- or tridentate-chelating ligands and provide the bridging function between the gadolinium atoms. It results in the formation of one-dimentional coordination polymers running along the *a* crystallographic direction in the crystal. The structure of $\{[Gd_2(CNCH_2COO)_6(H_2O)_4]\cdot 2H_2O\}$is shown in Fig. 2.

The Gd1···Gd2 and Gd1···Gd2′(*x-1,y,z*) separations within the 1D polymeric chains are equal to 4.7023(6) Å and 4.7245(6) Å, respectively. The polymeric structure is facilitated by four intramolecular H-bonds formed between coordinated water molecules and oxygen atoms from bidentate chelating carboxylate groups: O1*w*···O6(*1+x,1+y,z*) 2.863(10) Å, O1*w*-H···O6 2.06 Å, ∠O1*w*-H···O6 149°; O2*w*···O5 2.705(10) Å, O2*w*-H···O5 1.84 Å, ∠O2*w*-H···O5 161°; O3*w*···O1 2.695(11) Å, O2*w*-H···O1 1.84 Å, ∠O3*w*-H···O1 158°; O4*w*···O2(*-1+x,y,z*) 2.773(10) Å, O4*w*-H···O2 1.88 Å, ∠O4*w*-H···O2 155°. The packing of the structure can be characterized as a 3D network sustained by the numerous H-bonds formed between coordinated and solvate water molecules and nitrogen atoms of cyanoacetic groups: O1*w*···O5*w*(*x,-1+y,z*) 2.769(9) Å, O1*w*-H···O5*w* 1.87 Å, ∠O1*w*-H···O5*w* 174°; O2*w*···O6*w*(*x,-1+y,z*) 2.822(9) Å, O2*w*-H···O6*w* 1.96 Å, ∠O2*w*-H···O6*w* 159°; O3*w*···O5*w* 2.851(9) Å, O3*w*-H···O5*w* 2.00 Å, ∠O3*w*-H···O5*w* 156°; O4*w*···O6*w* 2.779(9) Å, O4*w*-H···O6*w* 1.87 Å, ∠O4*w*-H···O6*w* 174°; O5*w*···N1(*-1+x,y,z*) 2.99(1) Å, O5*w*-H···N1 2.16 Å, ∠O5*w*-H···N1 153°; O5*w*···N2(*1-x,-y,1-z*) 2.88(1) Å, O5*w*-H···N2 2.07 Å, ∠O5*w*-H···N2 150°; O6*w*···N3(*1+x,1+y,z*) 2.96(1) Å, O6*w*-H···N3 2.12 Å, ∠O6*w*-H···N3 155°; O6*w*···N6(*1-x,1-y,-z*) 2.94(1) Å, O6*w*-H···N6 2.10 Å, ∠O6*w*-H···N6 154°;

The Eu compound is isostructural to the Gd compound. Two non-equivalent sites for Eu are available, which are not identical but very similar to those in the Gd complex (Fig. S.1). For the sake of later comparison, we note that complexes **1** and **2** differ in the binding scheme with respect to the Nd compound **3**. In all cases, the cyano group of the cyanoacetate ligand is not coordinated to the lanthanide cation. However, the carboxylic groups exhibited different binding modes: 2-bidentate-chelating 2-bidentate and 2-tridentate-chelating bridging for **1** and **2**; while it is 2-bidentate and 2-tridentate-chelating bridging for complex **3**.

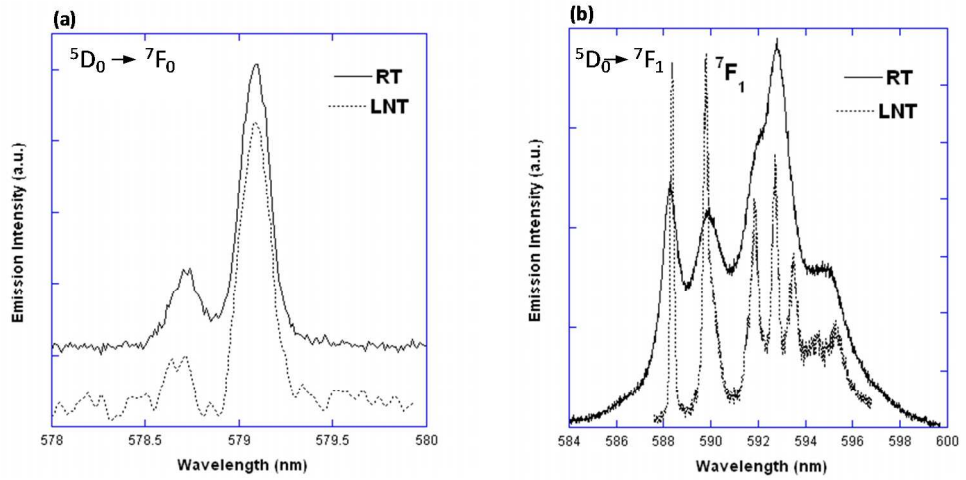

Fig. 3. Luminescence spectra of Eu complex **1** obtained at RT and 77 K: a) the $^5D_0 \rightarrow {}^7F_0$, b) the $^5D_0 \rightarrow {}^7F_1$ emission spectra.

In compound **3**, the Nd coordination consists of seven oxygen atoms originating from the carboxylate groups and two from water molecules, as in compounds **1** and **2**. Besides, the two Nd atoms in complex **3** are symmetry related, so both are equivalent, and thus just one type of coordination surrounding the Nd atom exists (Fig. S.1)..

3.3. Luminescence measurements

The magnetic properties of Eu(III) compounds are directly related to its optical ones, therefore, their determination are complementary in this work. Besides, Eu(III) is known [27] to yield a very intense luminescence spectrum, which, in turn, is very sensitive to the local symmetry of the site where the ion sits. Therefore, we have explored the luminescence spectrum of the europium compound **1**.

After the excitation with an excitation wavelength of 402 nm from the ^7F_o to the $^5D_3$ level, the system undergoes desexcitation from the $^5D_3$ to $^5D_0$, and subsequent radiative decay from $^5D_0$ to the ^7F_J low lying states. We show in Fig. 3(a) and (b) the $^5D_0 \rightarrow {}^7F_0$ and $^5D_0 \rightarrow {}^7F_1$ emission spectra, respectively, at room temperature and at 77 K. The presence of two $^5D_0 \rightarrow {}^7F_0$ bands is only compatible with the presence of two distinct sites for the Eu(III) ions. Moreover, the $^5D_0 \rightarrow {}^7F_1$ spectra is neatly resolved into a clearly split triplet (592-594 nm), and a second triplet, visible as a doublet with a second line depicting a shoulder. Besides, there is a spurious shoulder at low energies. This is clear evidence that the two distinct Eu sites determined from the X-ray diffraction experiments have different binding with the next neighboring ligands.

The average spin-orbit parameter, deduced from the energy difference between the center of mass of the ground state $^7F_0$ and the excited $^7F_1$ multiplets, gives the value λ_{opt}=360±10 cm^{-1}.

4. Thermo-magnetic properties

4.1. Eu complex (1)

A. Static magnetic properties

The Eu(III) ground state $^7F_0$ is non magnetic (L=3, S=3, J=0, g_J=0), however, it is split by the spin-orbit coupling into seven $S'L'J'$ states, with energies $E(J)=\lambda J(J+1)/2$, where λ is the spin-orbit coupling constant. Given that λ is relatively small, the crystal field (CF) components of the first $^7F_1$ and second $^7F_2$ excited states can be thermally populated. Hence, the mixture of $^7F_0$ with excited states ^7F_J, with J>1 and their thermal population give rise to paramagnetic response to the application of an external magnetic field, as we shall see.

The heat capacity (HC) at several applied fields, shown in Fig. 4, depicts a field independent lattice contribution down to 2

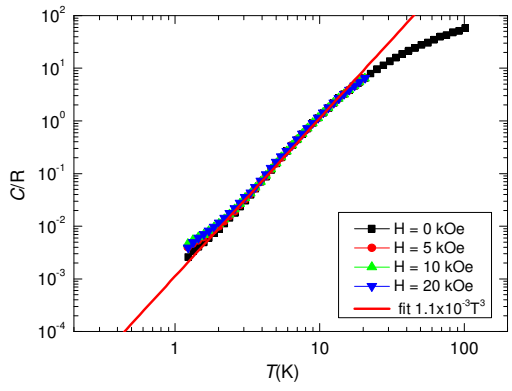

Fig. 4. Heat capacity of compound **1** at several applied fields.

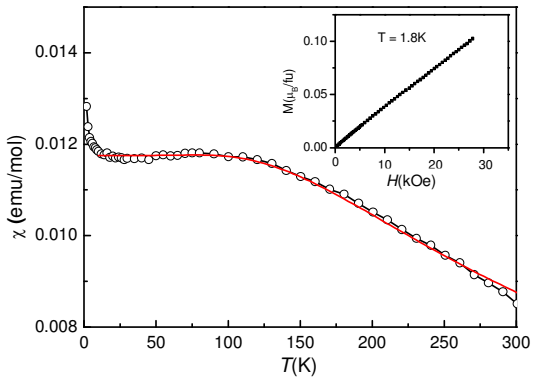

Fig. 5. Temperature dependence of the dc magnetic susceptibility of Eu complex **1**: (•) experimental data measured in an applied field H=200 Oe. (-) Fit obtained with the parameter λ=343 cm^{-1}. Inset: $M(H)$ measured at T=1.8 K.

K, and a very small magnetic contribution below. Since the latter is due to mixing of excited states, it is impossible to fit it to a simple model. So, we use this measurement essentially to determine the lattice contribution common to the series of compounds in this work. It was fitted by the Debye approximation at low temperature, $C_L^{LT} = AT^3$, with A/R=1.1x10^{-3} K^{-3}, and the Debye temperature is θ_D=240 K. From this parameter the average sound velocity in the system, calculated as:

$$c_s = (k_B/\hbar)\theta_D\left(6\pi^2 N/V\right)^{-1/3}, \quad [1]$$

where N is the number of molecules per unit cell, and V the cell volume, yielded c_s=2.04 x 10^{-3} m/s. We have used these values for the three compounds.

The experimental dc magnetic susceptibility χ_M of compound **1** measured from 0< T< 300 K in an applied field H=200 Oe is shown in Fig. 5. As temperature is lowered from room temperature, χ_M increases smoothly tending towards a plateau, with a value χ_M(LT)=1.17±0.02×10^{-2} emu/mol. A small increase at very low temperature is reminiscent of some spurious paramagnetic rare earth. The $M(H)$ measurements show, at T=1.8 K paramagnetic behavior, see Fig. 5 (inset), with a constant slope yielding to $\chi_M(T$=1.8K)=1.11±0.01×10^{-2} emu/mol. These features are common to many other europium(III) complexes [28].

The isotropic equilibrium magnetic susceptibility as a function of temperature at zero field χ_M of an Eu(III) ion has been developed with the van Vleck approximation in terms of λ as only fit parameter [28a]. From the fit of Eq. 8 in Ref. [28a], for a molecule containing two Eu(III) ions per formula unit, to the experimental data (see Fig. 5) the value λ=343±4 cm^{-1} is found. This determination of λ from powder magnetic data is not sensitive to the existence of two different europium sites. The obtained value is in good agreement with the average spin-orbit parameter deduced from the luminescence, λ_{opt}=360±10 cm^{-1}.

The $\chi_M(T$=1.8K) determined from the $M(H)$ measurement is in excellent agreement with the value obtained from $\chi_M(T)$ at the plateau; i.e. the paramagnetic impurity is saturated and does not hamper the slope determination from $M(H)$. It can be compared with the calculation based on the low temperature limit of χ_M, that relates it with the energies of the splitted excited triple state $^7F_1$, considering the $^7F_0$ as the ground state [28a], which for two different sites i=1,2 is expressed as:

$$(\chi_M)_{LT} \propto \sum_{i=1}^{2}\sum_{j=1}^{3} 1/E_j^i \, . \quad [2]$$

Using the energies of the main peaks in Fig. 3 (a) and (b), the value $(\chi_M)_{LT}$=1.18×10^{-2} emu/mol is obtained, in excellent agreement with the experimental result. One concludes that in this compound the Eu(III) valence state is stable.

4.2. Gd complex (2)

A. Static magnetic properties

The free Gd(III) ion ground state is a ^{8}S multiplet (L=0, S=7/2). In the absence of any perturbation, the ground state is spherically symmetric, i.e. isotropic upon the application of an external field. However, crystal field causes mixing of the ground state octet and excited sextets or even higher electronic levels giving rise to a Zero Field Splitting (ZFS) of the octet into four Kramers doublets [29, 30]. Thus, the distortion of the surrounding coordinating atoms determines the actual electronic level scheme.

The Hamiltonian describing this level splitting can be written as:

$$H_{ZFS} = D\left[S_z^2 - \frac{1}{3}S(S+1)\right] + E(S_x^2 - S_y^2), \quad [3]$$

where the axial, D, and orthorhombic, E, parameters can be experimentally determined. On the application of an external field the Zeeman term must be added:

$$H_Z = -g_J \mu_B H S_z \, . \quad [4]$$

The total Hamiltonian operates on the complete eight-fold basis function of the unperturbed wavefunction $|7/2, S_z\rangle$.

In principle, these constants could be determined from EPR spectra, however, the low temperature spectra (T=6 K) on powder performed at the X-band and at RT in the Q-band were featureless and no conclusive results could be obtained. In contrast, the magnetic heat capacity, C_m, at very low temperature is sensitive to this ZFS amounting to a few tenths of K since the

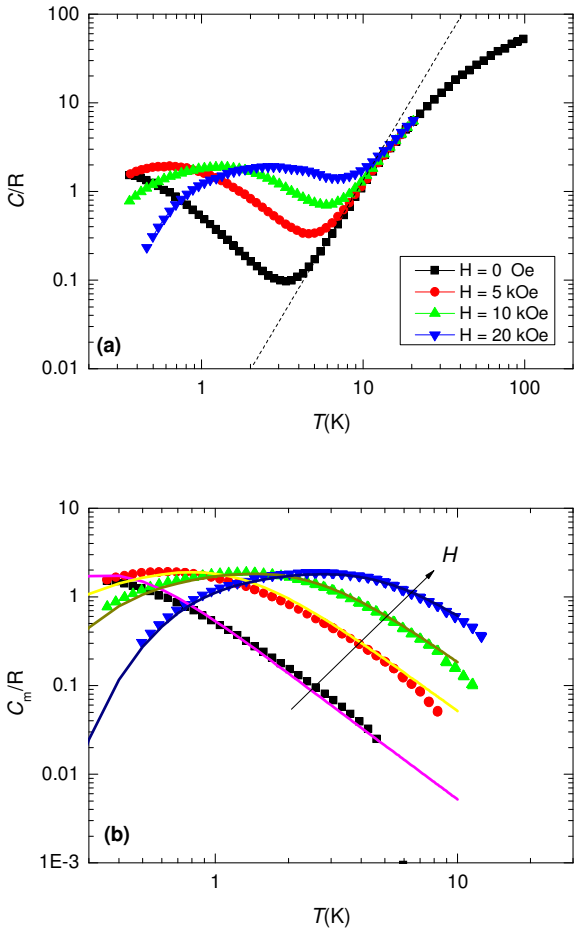

Fig. 6 a) Total low temperature HC of complex **2** powder measured at several applied fields. The dashed line corresponds to the lattice contribution, $C_L^{LT} = AT^3$, which is extrapolated at low temperature; b) Magnetic HC, $C_m(T, H)$, and fit to the predicted HC for a randomly oriented system of Gd(III) ions with parameters D/k$_B$=-0.11±0.01 K and E=0±0.03.

thermal population of the split levels gives rise to a Schottky type of rounded anomaly in the 1 K range.

In Fig. 6 the Heat Capacity (HC) data measured at magnetic fields H=0, 5, 10, 20 kOe are shown. Indeed, the magnetic anomalies are observable at low temperature, superimposed to the lattice contribution $C_L(T)$ which extends up to the highest measured temperature.

The lattice contribution dominating the heat capacity $C(H=0)$ above 4 K is in excellent agreement with that determined for compound **1** (Eu) (section 4.1 A), which has a negligible magnetic contribution. As the latter compound, it was fitted by the Debye approximation at low temperature, $C_L^{LT} = AT^3$, with A/R=1.1x10^{-3} K^{-3}.

After subtracting to lower temperatures the extrapolated $C_L(T)$ to the total $C(T)$ one obtains the magnetic HC curves, $C_m(T, H)$, which are shown in Fig. 6 (b).

The theoretical magnetic HC curves were calculated as follows: for a given orientation (θ, φ) of the magnetic field relative to the ion main axes, the single-ion Hamiltonian with uniaxial anisotropy and Zeeman term has been considered:

$$H_{si}(\theta,\varphi) = H_{CF} + H_{Zeeman} = DS_z^2 + E(S_x^2 - S_y^2) + g_J\mu_B H(\sin\theta\cos\varphi S_x + \sin\theta\sin\varphi S_y + \cos\theta S_z) \quad [5]$$

The heat capacity for a system of N=2N$_A$ magnetic atoms can be numerically calculated from the derivatives of the partition function $Z(\beta)$ for one Gd ion:

$$C(\theta,\varphi)/R = 2\beta^2\left[\frac{Z''*Z - Z'^2}{Z^2}\right], \quad [6]$$

with Z' and Z'' the first and second order derivatives with respect to $\beta=1/k_BT$ of the partition function corresponding to the above Hamiltonian. In a second step, the angular averaged specific heat for the powder sample is calculated as:

$$\bar{C}_m = \frac{\int_0^{2\pi} d\varphi \int_0^{\pi} C(\theta,\varphi)\sin\theta d\theta}{\int_0^{2\pi} d\varphi \int_0^{\pi} \sin\theta d\theta}. \quad [7]$$

The experimental curves have been fitted to the calculated heat capacity of a randomly oriented system of non-interacting Gd(III) ions subject to a ZFS with D/k_B=-0.11±0.01 K, E=0±0.03 K, and g_J=2.

The obtained D value is comparable in magnitude (though of opposite sign) to the value D/k_B=0.093 K and $|E|/k_B$ =0.007 K calculated by *ab initio* calculation methods in a Gd(III) ion with coordination nine, albeit of very different atoms [31]. This is a very small anisotropy, but, as we see below, has important consequences on the relaxation behavior of the compound.

The magnetocaloric effect (MCE) performance parameters have also been determined from the measured HC data. The magnetic entropy change $\Delta S_m(T, \Delta B_0)$ for selected field changes $\Delta B_0=\mu_0(H_f-H_i)$, see Fig. 7(a). A maximum final field H_f=20 kOe was chosen as to compare with other available data in the literature, where this field is taken as standard, since it is reachable with permanent magnets in the potential application as magnetic refrigerator. So, for ΔH=20 kOe the maximum value ΔS_m^{max} =64.9±1 mJ cm^{-3} K^{-1} is found at T^{max}=0.79 K. The full

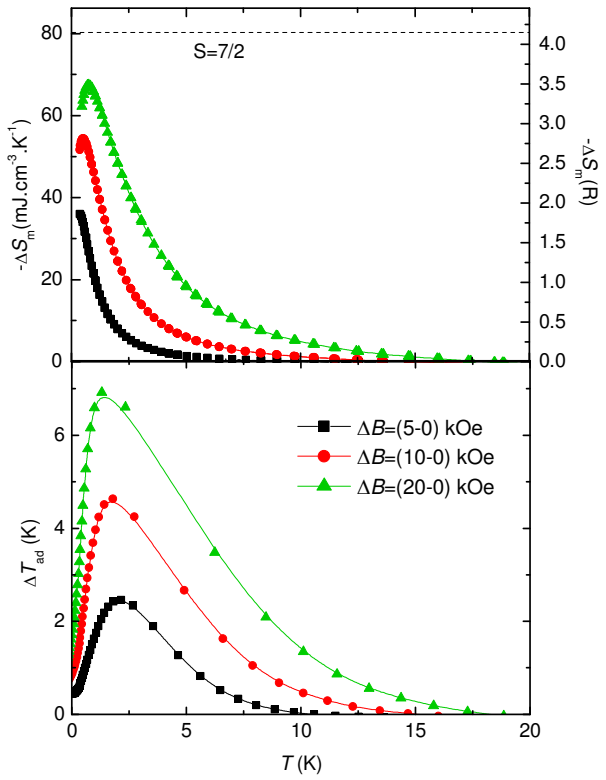

Fig. 7. Top: Temperature dependence of the magnetic entropy change, ΔS_m, as obtained from heat capacity data (Fig. 6) for the indicated applied-field changes ΔH. Left vertical axis units in volumetric mJ.cm^{-3} K^{-1}; right: units in R constants. Dashed line is the full entropy content for a S=7/2 spin system; b) Temperature dependence of the adiabatic temperature change $\Delta T_{ad}(T)$ as obtained from the heat capacity measurements.

width at half maximum of the ΔS_m curve is $\delta T_{FWHM} = 3.1K$ and the relative cooling power is $RCP = -\Delta S_m^{max} \times \delta T_{FWHM}$ =203.8 mJ cm^{-3}. Besides, the adiabatic temperature change $\Delta T_{ad}(T)=T_f-T_i$ has been calculated by solving the equation $S_m(T_f,\Delta H)-S_m(T_i,\Delta H)=0$ (Fig. 7(b)). For ΔH=20 kOe the temperature decrease at its maximum value is ΔT_{ad}^{max} =6.9 K at T=1.3 K.

These figures of merit are quite similar to those of [{Gd(OAc)$_3$(H$_2$O)$_2$}$_2$]·4H$_2$O (ρ=2.038 g cm^{-3}, ΔS_m^{max} =66.5±1 mJ cm^{-3} K^{-1}, T^{max}=0.9, $\delta T_{FWHM} = 3.2K$, RCP=212.8 mJ cm^{-3}, ΔT_{ad}^{max} =11.8 K at T=2 K) [32]. In both cases the Gd-Gd interaction is negligible. Let us note that in compound **2** T^{max} is slightly lower, thus more favorable, than those examples reported recently as candidates for MCE at very low temperatures [33].

The equilibrium dc magnetic susceptibility of gadolinium complex **2** was measured from 1.8 K to 300 K with a dc field of 1 kOe. The χT(300 K)=15.53±0.05 emu.K/mol and remains nearly independent of temperature down to 1.8 K (Fig. 8). There is no deviation from this line except for a small spurious peak due to some impurity at low temperature. It has been satisfactorily fitted with the model of two Gd(III) ions with L=0, S=7/2 isotropic spin, with g_J=2.0, predicting at RT χT(300 K)=15.76 emu.K/mol.

Isothermal magnetization curves, $M(H)$ have been measured at 1.8 K, 5 K and 10 K. The magnetization data represented as a function of the reduced applied field collapse into one curve, as

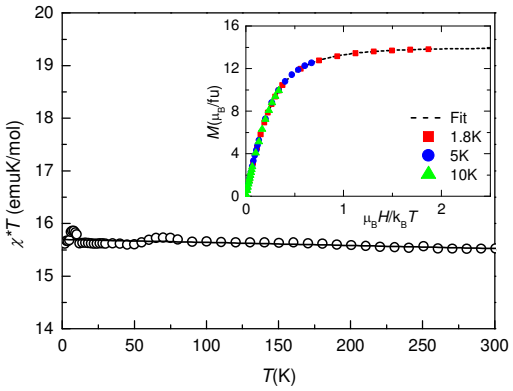

Fig. 8. Temperature dependence of the χT of Gd complex **2**: (•) experimental data measured in an applied field H=1 kOe. (-). Inset: Magnetization vs. the reduced applied magnetic field, $M(\mu_B H/k_B T)$ measured at T=1.8 K, 5 K and 10 K. (-) Fitted curve to S=7/2 multiplet (g_J=2.0).

shown in inset Fig.8. The isothermal $M(\mu_B H/k_B T)$ curve, measured at T=1.8 K was fitted with the same model of isotropic spin. No deviation from the Brillouin function for S=7/2 and g_J =2 was distinguishable, as could be expected for such a small anisotropy as D/k_B=-0.11 K. As can be seen in Fig. 8 (inset) the saturation magnetization amounts to M_s=14 μ_B/f.u. for two Gd ions per formula unit. In these measurements the two different sites for the Gd atom play no role.

Therefore, down to 1.8 K, no contribution from the Gd-Gd interaction can be distinguished within the dimeric molecule, or within the 1-D polymeric chain, in spite of Gd-Gd distance of the order of 4.7 Å. The tridentate chelate bridging (Gd1-Gd2) or the cyanoacetic acid bidentate bridge and H-bonds (Gd1-Gd2') do not seem to be efficient in generating any significant exchange interaction in the chain of gadolinium complex **2**. This is in contrast to, for example, μ-oxoacetate-bridged Gd complexes [34], where zig-zag chains with weakly ferromagnetic interaction via single-atom oxygen from the acetate groups were found, or the antiferromagnetic Gd-Gd interaction detected in the 2-D MOF $[Gd(HCOO)(OAc)_2(H_2O)_2]$, where the interaction takes place via single formato anti-anti bridges [35].

B. Dynamic properties: ac susceptibility

At H=0 and down to T=1.8 K, the ac susceptibility at different frequencies coincides with the equilibrium susceptibility. This implies that any relaxation process at H=0 is much faster than the highest frequency applied (f=1 kHz). The very small anisotropy energy of Gd in this complex cannot hinder spin reversal efficiently above 1.8 K.

However, as an external field is applied, both the in-phase $\chi'(T)$ and the out-of-phase component $\chi''(T)$ of the susceptibility show frequency dependence, indicating that the field enables slow relaxation processes. Figures 9a shows the ac susceptibility imaginary component $\chi''(f)$ data measured at H=2 kOe and different temperatures. From these data the relaxation time at different temperatures is obtained since $\chi''(T, f)$ has a maximum when the condition $\omega_{exp}\tau(T)$=1 is fulfilled (ω_{exp}=2πf).

It is noteworthy to observe that, at a given temperature, two χ'' maxima are measured at two different frequencies. The Cole-Cole plots of these experiments (see Supplementary material, Fig. S2 and S3) show too the existence of two clear slow relaxation processes: the first one, with a relaxation time τ_f~10^{-3} s, and a slower one with τ_s~0.2-1 s. Fig. 10 shows the ln $\tau(1/T)$ dependence of the two processes. The width of the time constants fall below α=0.4, thus there is a small distribution of constants evidently due to the fact that we are studying a powdered sample.

The physical scenario for Gd(III) is very different than for orthodox SIMs, since the anisotropy energy of Gd is very small ($\Delta_{ZFS}/k_B \approx$ 0.7 K), even lower than Zeeman splitting (Δ_H/k_B=1.9 K for M_s =7/2 at H=2 kOe).

The origin of the first process (τ_f) is not straightforward and needs from further discussion. This relaxation occurs in the whole measured temperature range, from 1.8 K to 10 K. One might assign it to a direct process ($\tau^{-1} \approx T$), however, this mechanism would not explain the experimental data in the whole temperature range. Moreover, the process cannot be assigned to an Orbach mechanism, since the energy value calculated from the ln $\tau_f(1/T)$ at 10 K, U/k_B=17 K, is orders of magnitude larger than the anisotropy barrier.

Nevertheless, the inverse of the faster relaxation time follows a $\tau_f^{-1} \propto T^2$ dependence (see Fig. 10 (b), inset). It has been recently proposed for a Gd complex [16] that such temperature dependence can be explained in terms of Resonant Phonon Trapping (RPT) mechanism [36, 37]. This process takes place when phonon-bottleneck effect sets on. Then the energy of the lattice modes created by the relaxing spins cannot be released into a thermal reservoir sufficiently fast. These phonons may be reabsorbed by other spins, and the effective relaxation time becomes longer.

For RPT to take place the system must fulfill some conditions [15, 37], namely: (i) spin-spin interactions must be rather weak,

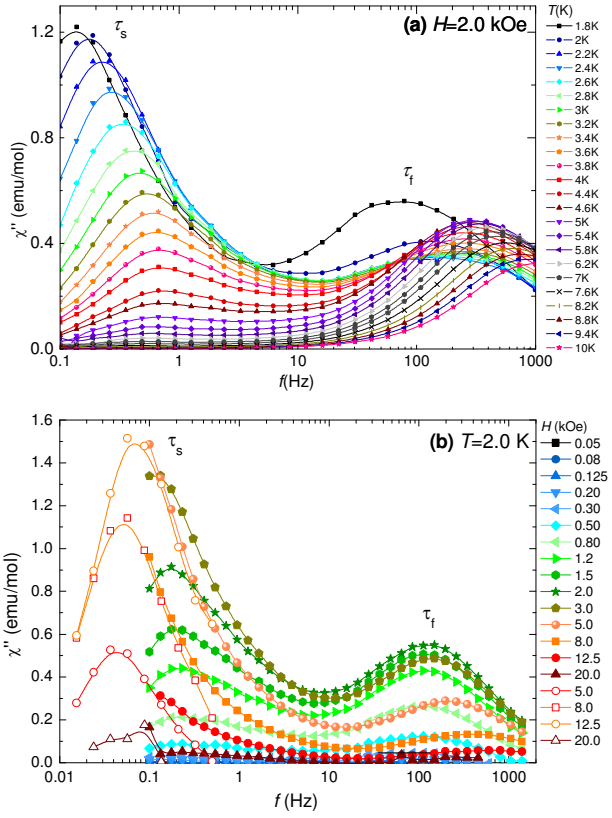

Fig. 9. Imaginary component of the ac susceptibility of complex **2** as a function of the frequency, $\chi''(f)$; a) $\chi''(T)$ at constant field H=2.0 kOe at different temperatures; b) at constant temperature T=2.0 K, at different applied fields.

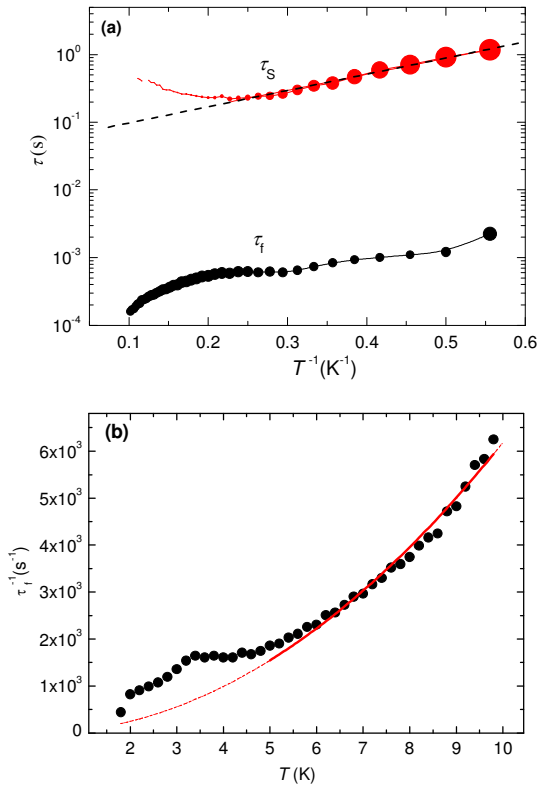

Fig. 10. a) Relaxation time as a function of the inverse temperature, $\tau(1/T)$, for complex **2**, at H=2 kOe. Slow process τ_f (black symbols) and slower one τ_s (red symbols). The size of each point is proportional to the height of the corresponding maximum; b) inverse of the faster slow relaxation time as a function of temperature, $\tau_f^{-1}(T)$. (Dashed line): Fit to $\tau_f^{-1}=KT^2$, with K=61.86 s^{-1} K^{-2} between 5 – 10 K.

so that energy transfer via the spin-spin interaction is not expected to be important; ii) at the temperature at which the very slow relaxation is observed the influence of thermal phonons may be neglected; and iii) the wavelength of the trapped phonons should be considerably larger than the typical separation between

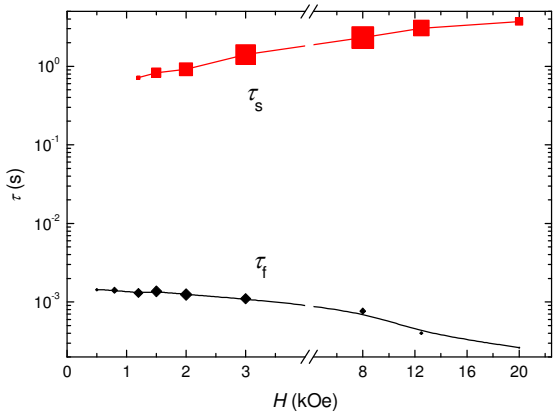

Fig. 11. Field dependence of the relaxation time for the two processes, $\tau_f(H)$ and $\tau_s(H)$, in Gd complex **2** at T=2.0 K, determined from the $\chi''(f)$ plots in Fig. 9b. The size of the symbols is proportional to the χ'' peak intensity.

the spins, $k_0 r_{av}$<<1, where r_{av} is the average distance between spin sites, and k_0 is the wave vector of the trapped phonon with the energy $h\nu_0$. Indeed, the difference between the splitted energy levels S_z=7/2 and S_z=-7/2 in a magnetic field of 2 kOe is ~1.9 K, therefore, using the Debye approximation $h\nu_0=c_s k_0$ and the average sound velocity obtained from the specific-heat data, it results k_0=1.9x10^7 m^{-1}. Taking into account that r_{av}≈4.7Å in this complex, the condition $k_0 r_{av}$≈9x10^{-3} <<1 is fulfilled. It may be concluded that the faster of the two relaxation processes in the Gd compound can be explained in terms of the RPT mechanism. The relaxation time τ_f is of the same order as that reported for the RPT process for the $Gd_2(fum)_3(H_2O)_4].3H_2O$ complex reported by Orendac [16].

The second observed slow process has relaxation time values in the order of τ_s≈0.1 to 1 s. The Kramers degeneracy of the Gd(III) ground state is lifted by the static field, resulting in a multi-level system with slow relaxation. In this case an Orbach and/or direct processes may govern the dynamics. Such a slow process is active mainly at low temperatures, where level splitting causes a thermal depopulation of all spin states and Orbach processes may take place. In fact, $\tau_s(1/T)$ could be fitted to an Arrhenius law with an activation energy of U/k_B=5.5 K, of the same order as the levels splitting (Δ_H/k_B=1.9 K). Similar values for a field induced relaxation in a Gd compound $[phen_2Gd_2(HCOO)_4(HCOO)_{2-2x}(NO_3)_{2x}]$ have been observed at H=2.75 kOe [13].

In order to study the evolution with the applied field of the two relaxation processes, we performed ac susceptibility measurements at constant T=2.0 K, at different fields (0.05 < H < 50 kOe) down to very low frequencies (0.02 < f < 10^3 Hz), see Figure 9b. The determined field dependence of the two relaxation paths is shown in Fig. 11. The very slow process $\tau_S(H)$ increases with field reaching a value of τ_s≈4 s at 20 kOe. As the slow relaxation follows an Arrhenius law with T, higher magnetic field implies larger activation energies and therefore longer relaxation times. The faster process, $\tau_f(H)$, on the contrary, decreases as field increases. That variation can be explained within the RPT mechanism. As levels energy splitting grows with magnetic field strength, the energy of involved phonons in RPT process increases and the condition $k_0 r_{av}$ <<1 is not so strongly fulfilled. Therefore, RPT is less effective as magnetic field increases and relaxation time decreases.

4.3. Nd complex (3)

A. Static magnetic properties

The neodymium cyanoacetate complex **3** [7] is not exactly isostructural to the europium and gadolinium complexes reported above. Though the Ln coordination is similar; i.e. by nine oxygen atoms, the 1-D linear chains are brought about by a not quite identical binding scheme. Besides, it has just one type of neodymium site, in contrast to the Eu or Gd. There are also two types of bridges; on one hand (Nd-Nd'), four cyanoacetic acid bidentate ligand, and, on the other hand (Nd-Nd''), through two tridentate chelate bridging anions of the cyanoacetic acid. Though strictly speaking, there is just one Nd per formula unit, we adhere to considering a duplicate formula unit to compare with the compounds **1** and **2**.

The Nd(III) has a free ion $^4I_{9/2}$ ground state (S=3/2, L=6, J=9/2), which is split by ligand field into five Kramers doublets. The lowest doublet is the only one populated at temperatures of the order of a few K [38].

Relativistic *ab initio* calculations were performed in order to determine the energy level structure of the Nd(III) multiplet

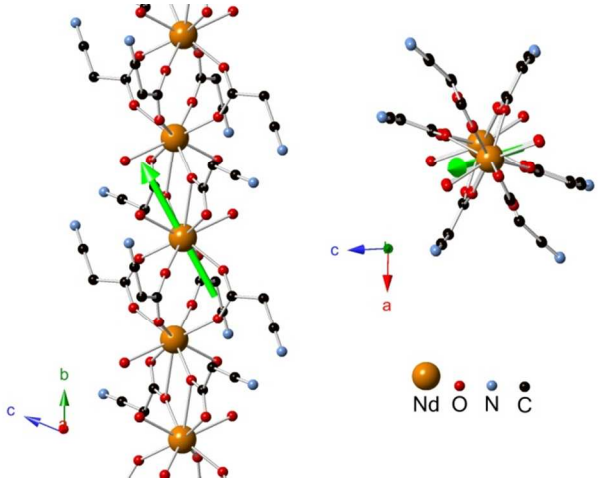

Fig. 12. Nd coordination environment and calculated direction of the easy axis of magnetization in complex **3**. Hydrogen atoms have been omitted for clarity.

ground state and the main axes of the g*-tensor for its doublet ground state, using the CASPT2/RASSI-SO [39] method as implemented in the MOLCAS 7.8 package [40]. This relativistic quantum-chemistry approach has proven suitable to analyse the magnetic anisotropy of lanthanide ions, and, in particular, to predict the direction of their easy axis of magnetization (EAM) [41]. The atomic positions were extracted from the x-ray crystal structure (see Figure 12). The cluster model includes the studied Nd ion and two La(III) ions in the positions of the two neighbour Nd(III) ions. The model also includes the cyanoacetic acid ligands and water molecules surrounding the studied Nd(III) ion and the water molecules surrounding the two neighbor Nd(III) ions. In order to reduce the computation time, without a significant loss of accuracy, the cyanoacetic acid ligands around the two neighour Nd(III) ions have been replaced by -0.5 point charges. The replacement of the neighour Nd(III) ion by an La(III) ion is done in order to reduce the active space. After that, the chosen CASSCF active space consisted of the Nd 4f orbitals, containing 3 electrons in seven orbitals [CASSCF(3,7)]. An averaged-state CASSCF calculation was done on the 4I quadruplets (13 roots) and then a CASPT2 correction was applied.

Ab initio calculations of the energies of the excited doublets have been performed, yielding the five Kramers doublets at the energies 0, 103.7, 276.1, 317.4 and 398.2 K i.e. the energy from the ground state to the first excited level is $\Delta_{ZFS}/k_B \approx 104$ K. The easy axis of magnetization is depicted in Fig. 12, and does not correspond to any of the site symmetry axes. The ground state doublet expressed in effective spin S*=1/2, g* factors are: $g_x^*=0.3$, $g_y^*=1.2$, $g_z^*=3.9$, where z is the principal axis of the g * tensor. It does not correspond to any principal crystallographic axis. Therefore, though the predominant anisotropy is along the z-axis, there is an important transversal component.

The Hamiltonian describing the quantum behavior of the system at low temperatures can be written in terms of the S*=1/2, anisotropic exchange interaction model:

$$H_{ex} = -2J_x^*\sum_{i,j}\left(S_{x,i}^*S_{x,j}^*\right) - 2J_y^*\sum_{i,j}\left(S_{y,i}^*S_{y,j}^*\right) - 2J_z^*\sum_{i,j}\left(S_{z,i}^*S_{z,j}^*\right). \quad [8]$$

Since the exchange constants J_a^* are proportional to g_a^{*2}, and $g_x^* \ll g_y^*$, then $J_x^2 < J_y^2 \ll J_z^2$ and the Hamiltonian can be reduced to

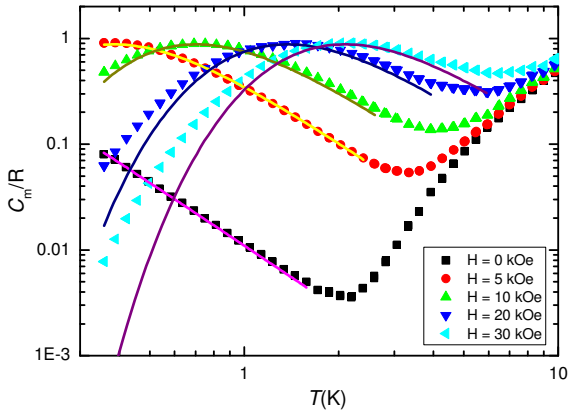

Fig. 13. HC of compound **3** at H=0 and other magnetic fields. For H=0, (dashed) fit of the HT tail of the exchange interaction. (Full lines) Schottky HC for average g_J^*=2.4.

two terms, a longitudinal term parallel to the z-axis, and a transversal term parallel to the y-axis.

Figure 13 shows the the heat capacity as a function of temperature measured at different fields. At H=0, the magnetic contribution to the low temperature HC is just a high temperature tail, $C_m/R=A_{ex}T^{-2}$ (A_{ex}=0.011 K^2), caused by the interaction to other Nd nearest neighbors. Hence, within this model the Nd-Nd interaction can be obtained since, within a mean field model [42], with S*=1/2 and for N=2N$_A$, since we consider 2 Nd per f.u:

$$A_{ext} = \frac{z}{4k_B^2}\left[J_x^2 + J_y^2 + J_z^2\right] \quad [9]$$

Assuming z=2 next Nd neighbors and $J_x^2 < J_y^2 \ll J_z^2$, one obtains an average value for the exchange interaction $|J_z| = 0.15$ K. Of course, we cannot determine the sign of this

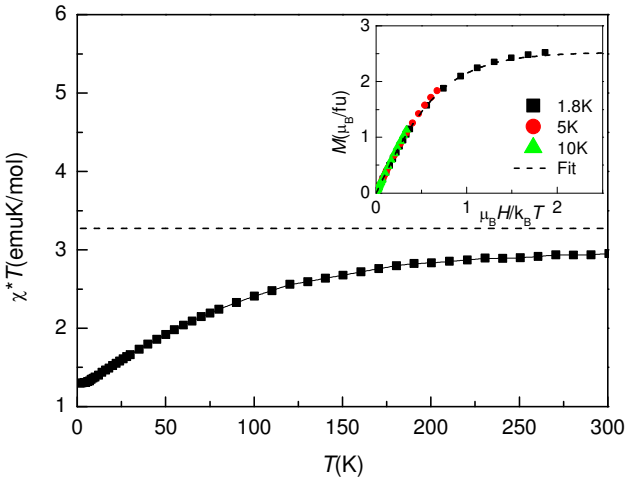

Fig. 14. Temperature dependence of the χT of Nd complex **3**: (•) experimental data measured in an applied field H=50 Oe. Dashed line: prediction for two free Nd ions. Inset: Magnetization vs. the reduced applied magnetic field, $M(\mu_BH/k_BT)$ measured at T=1.8 K, 5 K and 10 K. (-) Fitted curve to S*=1/2 doublet with ($g_x^*=g_y^*=1.8$, $g_z^*=3.7$).

interaction.

At $H\neq0$, clear Schottky type anomalies show up. They have been fitted to the predicted HC for a field split Kramers doublet with g_J*=2.4 in an effective spin S*=1/2 model. As the field increases, the experimental HC at the lowest temperatures is larger than the Schottky heat capacity. The difference can be assigned to a little broadening of the HC due to the angular random distribution of anisotropy axes.

The powder equilibrium dc susceptibility was measured from 1.8 to 300 K, and has been depicted in Fig. 14 as $\chi T(T)$. It decreases monotonically from the room temperature value χT(300K)=2.93(2) emu.K/mol. This value is already lower than the prediction for two independent free Nd(III) atoms per formula unit (χT=3.27 emu.K/mol). Its reduction as temperature decreases is the result of the thermal depopulation of the excited doublets.

Isothermal magnetization curves, $M(H)$ have been measured at 1.8 K, 5 K and 10 K. The reduced curves are almost superimposed, although a small deviation is detected at 10 K, where contribution from excited levels is slightly noticed (Inset Fig. 14).

At T=1.8 K the $M(H)$ curve obeys to an effective S^*=1/2 field dependence. It fits best to the prediction under the assumption of a ground doublet anisotropic with the average g*=2.4, after performing the angular averaging for a randomly oriented powder (see Fig. 14, inset). This value is near the g^*_{av}=1.8 obtained from the *ab initio* calculations. At any rate, the fully uniaxial anisotropy case ($g_x=g_y=0$, $g_z\neq0$) can be completely disregarded. The fit tensor parameters are similar to those found for Nd(III) diluted in La ethylsulfide complex, for example ($g_x^*=g_y^*$=2.072, g_z^*=3.535) [43]. In such a case, the ground doublet is composed of a combination of the $|9/2,\pm7/2\rangle$ and $|9/2,\pm5/2\rangle$ electronic states.

B. Dynamic properties: ac susceptibility

The dynamic behavior as a function of temperature and field has been studied by means of ac susceptibility measurements at varying frequency.

At H=0, no contribution to χ'' could be observed above 1.8 K, implying that there exists a relaxation process ($\tau<10^{-5}$ s) in this condition faster than the frequency window of our experiment ($0.01 < f < 10$ kHz).

Furthermore, we studied the dynamic behaviour under the application of magnetic fields. We performed frequency dependent ($0.1<f<10^4$ Hz) ac susceptibility measurements at different constant temperatures at H=1.5 kOe (this magnetic field was chosen because the $\chi''(f)$ intensity is maximum, as we shall see later). Figure 15a shows the $\chi''(f, T)$ data. The double-peaked $\chi''(f)$ curves evidence the existence of two different slow relaxation paths above 1.8 K, a faster one (τ_f) and a slower one (τ_s). The Cole-Cole plots of these experiments (see Supplementary material, Fig. S4 and S5) show too the existence of two clear slow relaxation processes. The width of the time constants fall below α=0.3, thus there is a small distribution of constants as in the Gd compound, due to the fact that we are measuring a powdered sample.

The relaxation time $\tau(1/T)$ dependence of the two existing processes has been deduced from the position of the $\chi''(T, f)$, see Fig. 16. The faster process τ_f (10^{-5} – 10^{-2} s) decreases continuously as the temperature is increased, tending to a continuous slope at the highest temperatures measured. From the slope of the $\tau_f(1/T)$ curve at high temperature an Arrhenius law with an activation energy value U/k_B=26.6(1) K is found for the Nd(III) ion, which is very small compared to the energy difference between the ground state and the first Kramers doublet (Δ_{ZFS}/k_B=104 K). The relaxation time of the other, very slow process is almost temperature independent $\tau_s\approx0.1$ s and gains intensity at low temperatures.

In order to study the evolution with the applied field of the two relaxation processes, we performed ac susceptibility measurements at constant T=2.0 K, at different fields ($0.05 < H < 50$ kOe) down to very low frequencies ($0.02 < f < 10^3$ Hz), see Figure 15b. The determined field dependence of the two relaxation paths is shown in Fig. 17. The faster process $\tau_f(H)$ is promoted by the field, it gains intensity and reaches a maximum $\tau_s\approx4.5\times10^{-3}$ s at 1.5 kOe and subsequently decreases with increasing field. Besides, the very slow process appearing for fields above 1.5 kOe, grows in amplitude and $\tau_s(H)$ is maximum at very high fields ($\tau_s\approx3$ s at 30 kOe).

The application of an external field has the effect of detuning the quantum tunneling process and allows the observation of the Orbach process already at low fields. The field strength at which this process appears gives us an estimation of the internal dipolar field. Indeed, as explained elsewhere [44], the tunneling time depends on the distribution of dipolar (or exchange) energy bias $P(\xi_{dip})$ and on the quantum tunnel splitting Δ_T:

$$\tau_{QT} \approx \frac{\hbar}{\Delta_T^2 P(\xi_{dip})}. \qquad [10]$$

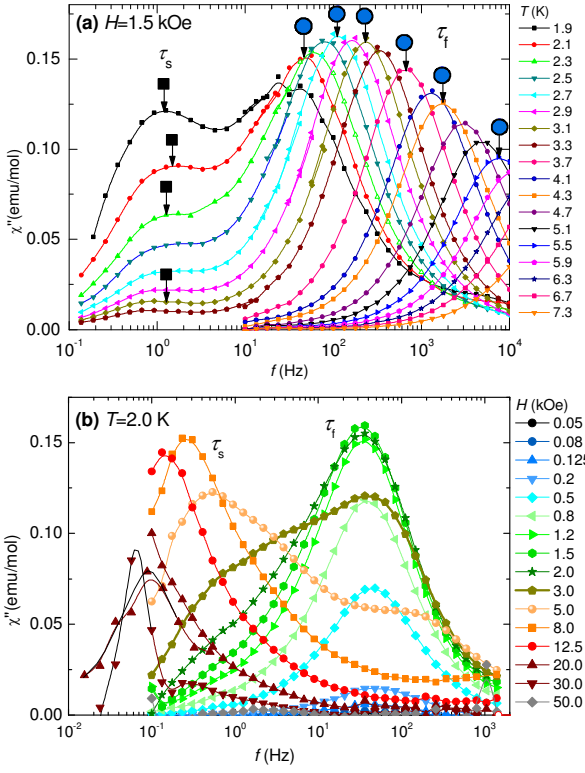

Fig. 15. Imaginary component of the ac susceptibility as a function of frequency, $\chi''(f)$; a): $\chi''(T)$ at constant field H=1.5 kOe at different temperatures; b) at constant temperature T=2.0 K, at different applied fields.

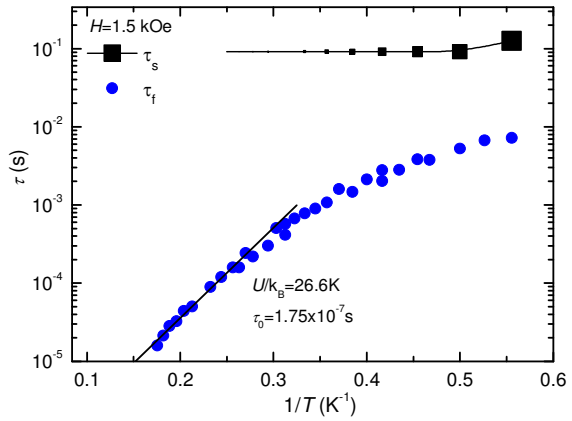

Fig. 16. Relaxation time as a function of the inverse temperature of relaxation processes found for Nd complex at H=1.5 kOe. The dependence of the two relaxation pathways, $\tau_f(1/T)$ and $\tau_s(1/T)$, determined from the $\chi''(f)$ plots in Fig. 15a are depicted. The size of the symbols reflects the decrease of intensity of the χ'' peak corresponding to the τ_s process. (-) Arrhenius law with activation energy U/k_B=26.6 K.

The energy bias distribution may be approximated to a Gaussian, with $P(\xi_{dip}=0)=1/\sqrt{2\pi}\sigma_{\xi dip}$, where the width $\sigma_{\xi dip}$ can be estimated from the condition $\sigma_{\xi dip} \approx k_B T_N$.

At $H\neq0$, the QT probability decreases as the Zeeman energy bias moves the tunneling energy window out of the dipolar energy bias distribution. We may consider that for an external field given by $H\approx2\sigma_{dip,z}$, QT is suppressed. The Orbach process appears at about 0.5 kOe. Therefore, the width of the bias field is estimated to be $\sigma_{dip,z}=H_{dip,z}\approx$250 Oe. For the Nd compound, this dipolar field would imply the magnetic ordering transition would occur at $K_B T_N = \sigma_{\xi dip} = \sigma_{dip,z}/g_z^*\mu_B \approx 0.06K$; this low value is in agreement with HC measurements, where ordering is not observed in $C_m(T)$ curves down to 0.35 K.

At H=0, the absence of $\chi''(T)$ within the measurement window implies that the QT relaxation time is faster than 10^{-5} s. Taking into account that the tunnel splitting, $\Delta_T = g^*_{xy}H_{dip,xy}$, this experimental threshold allows us as to give an estimation of lower limit of the transversal component of the dipolar field (Eq. [10]), $H_{dip,xy}$ > 19 Oe. Values for $H_{dip,xy}$ of similar strength as $H_{dip,z}$ would give QT times of 6 10^{-9} s, well beyond our frequency observation window.

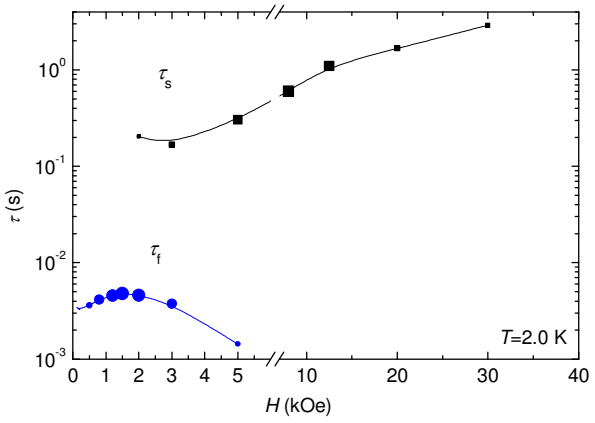

Fig. 17. Field dependence of the relaxation time for the two processes, $\tau_f(H)$ and $\tau_s(H)$, in Nd complex **3** at T=2.0 K, determined from the $\chi''(f)$ plots in Fig. 15b. The size of the symbols is proportional to the χ'' peak intensity.

In summary, two mechanisms cooperate in favoring fast tunneling at H=0: the non-zero dipolar field that splits the Kramers degeneracy and allows new relaxation pathways between the ground and the excited levels, on one hand, and the fact that in the present Nd(III) ion there is a quite remarkable transverse component in the g^* tensor. Therefore there may be an important relaxation in the transversal plane. The QT process is very effective and its relaxation time is short (τ_{QT}<1.6 x 10^{-5} s), below our frequency window. As a consequence, there is no χ'' contribution at the temperatures measured. This may be the reason for not observing slow relaxation at H=0 in most single-ion Nd complexes above 5 K [45]. There are some complexes containing Nd that show slow relaxation at H=0, however, in those examples the Nd moment is coupled to transition metal atoms in intermetallic clusters, so they do not belong to the class of SIM we are studying here [18-21].

The application of the external field has, as a first effect, the quenching of the QT mechanism. A second effect is the promotion of an Orbach type spin-lattice relaxation. In the temperature range above 3 K it yields to activation energy lower than Δ_{ZFS} [22]. In fact, Δ_{ZFS} would correspond to the highest limit for a thermally activated quantum tunneling (TAQT) activation energy only at H=0.

Besides, a second very slow process appears below 3 K, with relaxation time τ_s, which increases strongly in amplitude as the temperature decreases. This slow process is quite ubiquitous in many SIMs when a field is applied. We have identified it as the direct relaxation process via spin-phonon relaxation favoured by the lifting of the Kramers degeneracy by the application of the external field [8].

5. Conclusions

The lanthanide(III) cyanoacetate polymers of formula $\{[Ln_2(CNCH_2COO)_6(H_2O)_4]\cdot2H_2O\}_n$ where Ln= Eu (**1**), Gd (**2**), Nd (**3**) have been synthesized and characterized by single-crystal X-ray diffraction. Complexes **1** and **2** are isostructural and differ from the neodymium compound **3** structurally described earlier. In all cases, the cyano group of the cyanoacetate ligand is not coordinated to the lanthanide cation. The carboxylic groups exhibited different binding modes: bidentate-chelating, bidentate and tridentate-chelating bridging for **1** and **2**; bidentate and tridentate-chelating bridging for complex **3**. The three compounds have the similar tri-capped trigonal prism coordination of seven oxygen atoms from the carboxylate groups and two from water molecules.

The three compounds have conventional magnetic behavior in a static field: The Eu complex is paramagnetic, with the mixing of the ground state with excited levels governing its properties. Two different sites are discernible from luminescence measurements.

The paramagnetic Gd complex is almost isotropic, although a small anisotropic component has been found, caused by mixing of the excited states. There are two different Gd sites, but we could detect no site-dependent magnetic properties. From the heat capacity measurements the figures of merit as a magnetocaloric cooler have been determined, and we found complex **3** to be comparable to other Gd complexes where the Gd-Gd interaction is negligible.

In the Nd complex the Nd atoms are at equivalent sites. The Nd site is very anisotropic, with a predominantly uniaxial component, although a transverse component is also present.

Both Gd and Nd complexes have Kramers degenerate electronic states. In principle, the QT process should be forbidden for them. However, they show no slow relaxation at zero dc bias field, since a very fast relaxation process promotes equilibrium down to the lowest temperature measured (1.8 K). In the Gd case this fast process is of classical nature over a very small anisotropy barrier. In the Nd complex it can be explained in terms of a QT process favored by the transverse component in the anisotropy.

However, under the application of a high enough external field (H≈2 kOe) two slow relaxation processes are induced with relaxation times τ_f and τ_s. In the case of the nearly isotropic Gd complex, the small anisotropy plays no role in the observed relaxation. It is shown that $\tau_f \propto T^{-2}$, which is considered as a proof that resonant phonon trapping (RTP) is the cause of the spin slowing down because of the phonon-bottleneck effect. The slow process becomes more intense at the expense of the fast one, which is interpreted as due to Orbach relaxation processes between ground and excited states, favored by the lifting of the Kramers degeneracy by the external field.

In contrast, for the Nd compound the fast relaxation process is accounted for by an Orbach type spin-lattice relaxation with τ_f governed by an activation energy that decreases with decreasing temperature. The slow component τ_s seems to be caused by direct relaxation processes with Kramers split excited levels.

Direct and Orbach processes under an applied fields have been detected by means of EPR measurements to occur in Nd compounds already in the 60's [46]. In those experiments an average relaxation time was measured. Improving on that result, in the present experiments the two relaxation times are actually resolved.

We conclude that both the Gd and Nd complexes present slow relaxation only when an external field is applied, albeit with a quite different relaxational behavior mechanism. The Gd complex can be satisfactorily described in terms of the RTP mechanism, and thus, described as a SIM. Besides, there have been reported only a few neodymium containing clusters, with slow relaxation processes, described as SMMs. We would like to emphasize that in the present Nd complex, slow relaxation is solely caused by the only magnetogenic atom, Nd, which behaves as a SIM. This finding deserves a deeper on-look to homonuclear Nd complexes as SIMs.

Acknowledgements

This work has been financed by MECOM Projects MAT11/23791, MAT11/27233-C02-02, DGA Projects E34 Consolider Nanoselect (CSD2007-00041) and Aplicative Institutional Project 11.817.08.24A (ICh ASM). The authors thankfully acknowledge the resources from the supercomputer "Caesaraugusta" (node of the Spanish Supercomputer Network), technical expertise and assistance provided by BIFI - Universidad de Zaragoza. Authors would like to acknowledge the use of Servicio General de Apoyo a la Investigación-SAI, Universidad de Zaragoza. Drs. A. Camón and P. Alonso, of ICMA, are thanked for complementary measurements.

References

1 C. Benelli and D. Gatteschi, *Chem.Rev*., 2002, **102**, 2369.
2 Y. Hasegawa, T. Nakagawa, T. Kawai, *Coord. Chem. Rev*., 2010, **254**, 2643.
3 (a) K.-L. Hou, F.-Y. Bai, Y.-H. Xing, J.-L. Wang, Z. Shi, Inorg. *Chim. Acta*, 2011, **365**, 269; (b) J. Fan, Z.-H. Wang, Z.-F. Huang, X. Yin, W.-G. Zhang, *Inorg. Chem. Commun*., 2010, **13,** 659; (c) Y. Tang, K.-Z. Tang, J. Zhang, C.-Y. Su, W.-S. Liu, M.-Y. Tan, *Inorg. Chem. Commun*., 2005, **8**, 1018; (d) D.-L. Long, A.J. Blake, N.R. Champness, C. Wilson, M. Schroder, *Angew. Chem. Int. Ed*., 2001, **40**, 2443; (e) T.M.Reineke, M.Eddaoudi, D.Moler, M. O'Keeffe, O.M.Yaghi, *J. Am. Chem. Soc*., 2000, **122**, 4843.
4 (a) X.-D. Yang, C.-H. Zhang, D.-P. Wang, Y.-G. Chen, *Inorg. Chem. Commun*., 2010, **13**, 1350; (b) H.-B. Zhang, Y.Peng, X.-C. Shan, C.-B. Tian, P. Lin, S.-W. Du, *Inorg. Chem. Commun*., 2011, **14**, 1165; (c) J. P. Costes, J.M.C. Juan, F. Dahan, F. Nicodème, *Dalton Trans*., 2003, **7,** 1272; (d) R. Gheorghe, V. Kravtsov, Yu. A. Simonov, J.-P. Costes, Y. Journaux, M. Andruh, *Inorg. Chim. Acta*, 2004, **357**, 1613; (e) X.-J. Zheng, Z.-M. Wang, S.Gao, F.-H. Liao, C.-H.Yan, L.-P. Jin, *Eur. J. Inorg.Chem*., 2004, **14**, 2968.
5 (a) P. Starynowicz, *Acta Crystallografica, Sect. C*, 1993, **C49**, 1621; (b) P. Starynowicz, *Pol. J. Chem.,* 1994, **68**, 621.
6 G. Novitskii, S. Shova, V. Voronkova, L. Korobchenko, M. Gdanek, Iu. Simonov, C. Turta, *Russ. J. Coord.Chem*., 2001, **7**, 791.
7 S. G. Shova, Yu. A. Simonov, M. Gdaniec, G. V. Novitchi, A. Lazarescu, K. I. Turta., *Russ. J. Inorg. Chem*., 2002, **47**, 946.
8 E. Bartolomé, J. Bartolomé, S. Melnic, D. Prodius, S.Shova, A. Arauzo, J. Luzón, F. Luis and C. Turta, *Dalton Trans*., 2013, **42**, 10153.
9 R. Sessoli and A.K. Powell, *Coord. Chem. Rev.*, 2009, **253**, 2328.
10 L. Bogani, C. Sangregorio, R. Sessoli and D. Gatteschi, *Angew. Chem. Int. Ed*., 2005, **44**, 5817.
11 X. Feng, J. Liu, TD. Harris, S. Hill and J.R. Long, *J. Am. Chem. Soc*., 2012, **134**, 7521.
12 J.M. Zadrozny, J. Liu, N.A. Piro, Ch.J. Chang, S. Hilland J.R. Long, *Chem. Comm*., 2012, **48**, 2927.
13 B. Liu, B-W. Wang, Z-M. Wang and S. Gao, *Sci. China, Chem*., 2012, **5,** 926.
14 M. J. Martínez-Pérez, S. Cardona-Serra, C. Schlegel, F. Moro, P. J. Alonso, H. Prima-García, J. M. Clemente-Juan, M. Evangelisti, A. Gaita-Ariño, J. Sesé, J. van Slageren, E. Coronado, and F. Luis, *Phys. Rev. Lett.* 2012, **108**, 247213.
15 M. Fang, J-J. Li, P-F. Shi, B. Zhao and P. Cheng, *Dalton Trans*., 2013, **42**, 6553.
16 M. Orendáč, L. Sedláková, E. Čižmár, A. Orendáčová, A. Feher, S. A. Zvyagin and J. Wosnitza, W. H. Zhu, Z. M. Wang, and S. Gao, *Phys. Rev. B*, 2010, **81**, 214410.
17 M. Evangelisti, in *Molecular magnets: Physics and Applications*, Eds. J. Bartolomé, F. Luis, J.F. Fernández, Springer Series on *Nanoscience and Nanotechnoloy*, 2013, Ch. 14, 365.
18 H. Ke, L. Zhao, Y. Guo and J. Tang, *Dalton Trans*., 2012, **41**, 2314.
19 V. Mereacre, D. Prodius, A.M. Ako, N. Kaur, J. Lipkowski, Ch. Simmons, N. Dalal, I. Geru, Ch. E. Anson, A. K. Powell and C. Turta, *Polyhedron*, 2008, **27**, 2459.
20 A. Mishra, W. Wernsdorfer, K. A. Abboud and G. Christou, *J. Am. Chem. Soc*., **126**, 15648 (2004).
21 M-X. Yao, Q. Zheng, K. Qian, Y. Song, S. Gao, and J-L. Zuo, *Chem. Eur. J*., 2013, **19**, 294.
22 P. Vrábel, M. Orendáč, A. Orendáčová, E. Čižmár, R. Tarasenko, S. Zvyagin, J. Wosnitza, J. Prokleska, V. Sechovský, V Pavlík and S. Gao, J. *Phys.: Condens. Mat.*, 2013, **25**, 186003.

23 K. Nakamoto, *Infrared and Raman Spectra of Inorganic and CoordinationCompounds*, A Wiley-Interscience Publ. John Wiley and Sons, New York, Chichester, Brisbane, Toronto. Singapore, 1991, 504p. (transl. in rus.).

24 CrysAlis RED, Oxford Diffraction Ltd.,Version 1.171.34.76, 2003.

25 G. M. Sheldrick, SHELXS-97. Program for Crystal Structure Solution. Univ. of Göttingen: Göttingen, Germany, 1990.

26 G. M. Sheldrick, SHELXL-97. Program for the refinement of crystal structures from diffraction data. Univ. of Göttingen: Göttingen,Germany, 1997.

27 R. Reisfeld, in *Structure and Bonding*, Rare Earth Series 1975, Vol. **22**, 123.

28 (a) M. Andruh, E. Bakalbassis, O. Kahn, J. Ch. Trombe, P. Porchers, *Inorg. Chem*., 1993, **32**, 1616; (b) B. Barja, P. Aramendia, R. Baggio, M.T. Garland, O. Peña, M. Perec. *Inorg. Chim. Acta*, 2003, **355**, 183; (c) C. Turta, S. Melnic, M. Bettinelli, S. Shova, C. Benelli., A. Speghini, A. Caneschi, M. Gdaniec, Yu. Simonov, D. Prodius, V. Mereacre, *Inorg. Chim. Acta*, 2007, **360**, 3047; (d) J. Legendziewicz and M. Borzechowska, *J. of Alloys and Comp*., 2000, **300-301,** 353.

29 B.G. Wybourne, *Phys. Ver*. 1966, **148**, 317.

30 D. J. Newman W. Urban, *Adv. Phys.*, 1975, **24**, 793.

31 M. Ferbinteanu, F. Cimpoesu, M. A. Girtu, C. Enachescu and S. Tanase, *Inorg. Chem*., 2012, **51**, 40.

32 M. Evangelisti, O. Roubeau, E. Palacios, A. Camón, T. N. Hooper, E.K. Brechin, and J.J. Alonso, *Angew. Chem. Int. Ed*. 2011, **50**, 6606.

33 G. Lorusso, J.W. Sharples , E. Palacios, O. Roubeau , E.K. Brechin, R. Sessoli, A. Rossin , F. Tuna , E.J.L. McInnes , D. Collison , and M. Evangelisti, *Adv. Mater*, 2013, **25**, 4653.

34 F-Sh. Guo, J-D. Leng, J-L. Liu, Z-Sh. Meng, and M-L. Tong, *Inorg. Chem*., 2012, **51**, 405.

35 G. Lorusso, M. A. Palacios, G. S. Nichol, E. K. Brechin, O. Roubeau and M. Evangelisti, *Chem. Commun*., 2012, **48**, 7592.

36 R. Schenker, M. N. Leuenberger, G. Chaboussant, D. Loss, and H. U. Güdel, *Phys. Rev. B*, 2005, **72**, 184403.

37 D. L. Huber, *Phys. Rev. B*, 1965, **139**, A1684.15.08.2013.

38 R.L. Carlin, in *Magnetochemistry*, Springer-Verlag (Berlin Heidelberg New York, Tokyo, 1986.

39 B. O. Roos and P. A. Malmqvist, *Phys. Chem. Chem. Phys.,* 2004, **6**, 2919.

40 F. Aquilante, L. De Vico, N. Ferre, G. Ghico, P. A. Malmqvist, P. Neogrady, T. B. Pedersen, M. Pitonak, M. Reiher, B. O. Roos, L. Serrano-Andres, M. Urban, V. Veryazov and R. Lindh, *J. Comp. Chem.,* 2010, **31**, 224.

41 K. Bernot, J. Luzon, L. Bogani, M. Etienne, C. Sangregorio, M. Shanmugam, A. Caneschi, R. Sessoli and D. Gatteschi, *J. Am. Chem. Soc.,* **131**, 5573 (2009); G. Cucinotta, M. Perfe, *Nat. Chem.*, 2011, **3**, 538.

42 T. deNeef and J.P.A.M. Hijmans, *J. Phys. A. Math. Gen*. 1976, **9**, 1.

43 A. Abragam and B. Bleaney, in *Electron Paramagnetic resonance of transition ions*, Oxford University Press, 1970, p. 306.

44 (a) N.V. Prokof'ev and P.C.E. Stamp, *Phys. Rev. Lett*., 1988, **80**, 5794; (b) W. Wernsdörfer, T. Ohm, C. Sangregorio, R. Sessoli, D. Mailly, C. Paulsen, *Phys. Rev. Lett*., 1999, **82**, 3903.

45 (a) A.M. Ako, V. Mereacre, R. Clérac, I. J. Hewitt, Y. Lan, G. Buth, C. E. Anson and A. K. Powell, *Inorg. Chem*., 2009, **48**, 6713; (b) P. C. Andrews, T. Beck, B. H. Fraser, P. C. Junk, M. Massi, K. S. Murray and M. Silberstein, *Polyhedron*, 2009, **28**, 2123; (c) V. Chandrasekhar, B. M. Pandian, R. Boomishankar, A. Steiner, J. J. Vittal, A. Houri and R. Clérac, *Inorg. Chem*., 2008, **47**, 4918; (d) H. L. C. Feltham, F. Klower, S. A. Cameron, D. S. Larsen, Y. Lan, M. Tropiano, S. Faulkner, A. K. Powell and S. Brooker, *Dalton Trans*., 2011, **40**, 11425; (e) S. Y. Liao, W. Gu,L-Y. Yang,T.-H. Li, J.-L. Tian,L. Wang,M. Zhang and X. Liu, *Cryst. Growth Des*., 2012, **12**, 3927; (f) J. Liu, C. Ma, H. Chen, M. Hu, H. Wen, H. Cui, X. Song and C. Chen, *Dalton Trans*., 2013, **42**, 2423; (g) V. Mereacre, Y. Lan, R. Clérac, A. M. Ako, W. Wernsdorfer, G. Buth, C. E. Anson and A. Powell, *Inorg. Chem*., 2011, **50**, 12001; (h) V. Mereacre, Y. Lan, R. Clérac, A. M. Ako, I. J. Hewitt, W. Wernsdorfer, G. Buth, C. E. Anson and A. K. Powell, *Inorg. Chem*., 2010, **49**, 5293; (i) S. Nayak, O. Roubeau, S. J. Teat, C. M. Beavers, P. Gamez and J. Reedijk, *Inorg. Chem*., 2010, **49**, 216; (j) T. D. Pasatoiu, J.-P. Sutter, A. M. Madalan, F. Z. C. Fellah, C. Duhayon and M. Andruh, *Inorg. Chem*. 2011, **50**, 5890; (k) J. -B. Peng, Y.- P. Ren, X. –J. Kong, L. –S. Long, R. –B. Huang and L. –S. Zheng, *Cryst. Eng. Comm*., 2011, **13**, 2084; (l) D.T. Thieleman, M. Klinger, T. J. A. Wolf, Y. Lan, W. Wernsdorfer, M. Busse, P. W. Roesky, A. N. Unterreiner, A. K. Powell, P. C. Junk and G. B. Deacon, *Inorg. Chem.* 2011, **50**, 11990; (m) Y. Wang, X.-L. Li, T. –W. Wang, Y. Song and X. –Z. You, *Inorg. Chem.* 2010, **49**, 969; (n) W.-H. Yan, S.-S. Bao, L.-L. Ding, C. –S. Lu, Q.-J. Meng, L.-M. Zheng, *Inor. Chem*.,2013, **28**, 20; (o) J. M. Zhou, W. Shi, N. Xu and P. Cheng, *Cryst. Grow. Des*. **13**, 1218; (p) A. Baniodeh, Y. Lan, G. Novitchi, V. Mereacre, A. Sukhanov, M. Ferbinteanu, V. Voronkova, C. E. Anson and A. K. Powell, *Dalton Trans*., 2013, **42**, 8926; (q) X. Feng, Y.-Q. Feng, L. Liu, L.-Y. Wang, H.-L. Song and S. –W. Ng, *Dalton Trans*., 2013, **42**, 7741; (r) L. Tian, Y. -Q. Sun, B. Na, P. Cheng, *Eur. J. Inor. Chem*., 2013, **24**, 4329; (s) M. Fang, Z. Ming, H. H. Zhao, A. V. Prosvirin, D. Pinkowicz, B. Zhao, P. Cheng, W. Wernsdorfer, E. K. Brechin, K. R. Dunbar, *Dalton Trans*., 2013, **42**, 14693.

46 R. H. Ruby, H. Benoit, and C.D. Jeffies, *Phys. Rev.* 1962, **127**, 51.

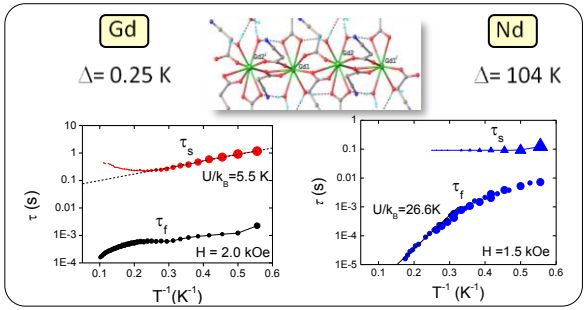

The cyanoacetate complexes, $\{[Ln_2(CNCH_2COO)_6(H_2O)_4]\cdot 2H_2O\}_n$, with Ln= Gd, Nd, show field-induced slow relaxation ascribed to two different processes: Resonant Phonon Trapping and lifting of the Kramers degeneracy on the ground state for Gd, and an Orbach and direct processes for Nd.